IJMMM International Journal of Minerals, Metallurgy and Materials 矿物冶金与材料学报（英文版）

Layered barium vanadate nanobelts for high-performance aqueous zinc-ion batteries

Xing-hua Qin, Ye-hong Du, Peng-chao Zhang, Xin-yu Wang, Qiong-qiong Lu, Ai-kai Yang, and Jun-cai Sun

Cite this article as:
Xing-hua Qin, Ye-hong Du, Peng-chao Zhang, Xin-yu Wang, Qiong-qiong Lu, Ai-kai Yang, and Jun-cai Sun, Layered barium vanadate nanobelts for high-performance aqueous zinc-ion batteries, *Int. J. Miner. Metall. Mater.*, 28(2021), No. 10, pp. 1684-1692. https://doi.org/10.1007/s12613-021-2312-4

View the article online at SpringerLink or IJMMM Webpage.

Articles you may be interested in

Mohammad Sefidmooy Azar, Shahram Raygan, and Saeed Sheibani, Effect of chemical activation process on adsorption of As(V) ion from aqueous solution by mechano-thermally synthesized zinc ferrite nanopowder, *Int. J. Miner. Metall. Mater.*, 27(2020), No. 4, pp. 526-537. https://doi.org/10.1007/s12613-019-1931-5

Toyohisa Fujita, Hao Chen, Kai-tuo Wang, Chun-lin He, You-bin Wang, Gjergj Dodbiba, and Yue-zhou Wei, Reduction, reuse and recycle of spent Li-ion batteries for automobiles: A review, *Int. J. Miner. Metall. Mater.*, 28(2021), No. 2, pp. 179-192. https://doi.org/10.1007/s12613-020-2127-8

Kai-lin Cheng, Dao-bin Mu, Bo-rong Wu, Lei Wang, Ying Jiang, and Rui Wang, Electrochemical performance of a nickel-rich $LiNi_{0.6}Co_{0.2}Mn_{0.2}O_2$ cathode material for lithium-ion batteries under different cut-off voltages, *Int. J. Miner. Metall. Mater.*, 24(2017), No. 3, pp. 342-351. https://doi.org/10.1007/s12613-017-1413-6

Li-fen Guo, Shi-yun Zhang, Jian Xie, Dong Zheng, Yuan Jin, Kang-yan Wang, Da-gao Zhuang, Wen-quan Zheng, and Xin-bing Zhao, Controlled synthesis of nanosized Si by magnesiothermic reduction from diatomite as anode material for Li-ion batteries, *Int. J. Miner. Metall. Mater.*, 27(2020), No. 4, pp. 515-525. https://doi.org/10.1007/s12613-019-1900-z

Azhar Iqbal, Long Chen, Yong Chen, Yu-xian Gao, Fang Chen, and Dao-cong Li, Lithium-ion full cell with high energy density using nickel-rich $LiNi_{0.8}Co_{0.1}Mn_{0.1}O_2$ cathode and SiO-C composite anode, *Int. J. Miner. Metall. Mater.*, 25(2018), No. 12, pp. 1473-1481. https://doi.org/10.1007/s12613-018-1702-8

Hendrik Setiawan, Himawan Tri Bayu Murti Petrus, and Indra Perdana, Reaction kinetics modeling for lithium and cobalt recovery from spent lithium-ion batteries using acetic acid, *Int. J. Miner. Metall. Mater.*, 26(2019), No. 1, pp. 98-107. https://doi.org/10.1007/s12613-019-1713-0

IJMMM WeChat

QQ author group

International Journal of Minerals, Metallurgy and Materials
Volume 28, Number 10, October 2021, Page 1684
https://doi.org/10.1007/s12613-021-2312-4

Layered barium vanadate nanobelts for high-performance aqueous zinc-ion batteries

Xing-hua Qin[1)], *Ye-hong Du*[1)], *Peng-chao Zhang*[1)], *Xin-yu Wang*[1)], *Qiong-qiong Lu*[2)], *Ai-kai Yang*[3)], *and Jun-cai Sun*[1)]

1) Institute of Materials and Technology, Dalian Maritime University, Dalian 116026, China
2) Institute for Complex Materials, Leibniz Institute for Solid State and Materials Research (IFW) Dresden e.V., Helmholtzstraße 20, 01069 Dresden, Germany
3) Materials Synthesis and Processing (IEK-1), Institute of Energy and Climate Research, Forschungszentrum Jülich GmbH, 52425 Jülich, Germany
(Received: 5 April 2021; revised: 31 May 2021; accepted: 4 June 2021)

Abstract: Aqueous zinc-ion batteries (ZIBs) are deemed as the idea option for large-scale energy storage systems owing to many alluring merits including low manufacture cost, environmental friendliness, and high operations safety. However, to develop high-performance cathode is still significant for practical application of ZIBs. Herein, $Ba_{0.23}V_2O_5{\cdot}1.1H_2O$ (BaVO) nanobelts were fabricated as cathode materials of ZIBs by a typical hydrothermal synthesis method. Benefiting from the increased interlayer distance of 1.31 nm by Ba^{2+} and H_2O pre-intercalated, the obtained BaVO nanobelts showed an excellent initial discharge capacity of 378 $mAh{\cdot}g^{-1}$ at 0.1 $A{\cdot}g^{-1}$, a great rate performance (e.g., 172 $mAh{\cdot}g^{-1}$ at 5 $A{\cdot}g^{-1}$), and a superior capacity retention (93% after 2000 cycles at 5 $A{\cdot}g^{-1}$).

Keywords: aqueous zinc-ion batteries; barium vanadate nanobelts; increased interlayer distance; long cycle life

1. Introduction

Lithium-ion batteries (LIBs) have been wildly applied to provide energy for a variety of devices in recent decades due to their splendid energy/power density and supernormal life span [1–2]. However, the potential applications of such batteries in large-scale energy storage systems are seriously hindered by the shortage of lithium metal resources, exorbitant cost, harsh preparation conditions, and safety hazards [3–5]. Rechargeable aqueous batteries using the aqueous electrolyte with high ionic conductivity, as alternative systems to LIBs, have attracted widespread attention [6–8]. Among these systems, aqueous zinc-ion batteries (ZIBs) triggered more attention not only because they are environmental friendliness, high operations security, and low manufacture cost, but also because they are involved chemistry with a two-electron transfer mechanism [9–10]. Furthermore, zinc metal anode possesses the outstanding merits of great abundance, low redox potential, and excellent theoretical capacity [11–14]. These remarkable advantages make aqueous ZIBs to be a potential energy storage solution for large-scale energy storage systems. Nonetheless, developing admirable performance cathode materials to meet the practical application requirements of ZIBS remains a huge challenge.

In recent years, various cathode materials are developed and mainly concentrated on the V-based materials with multiple oxidation states, Prussian blue analogs with open-frame construction, Mn-based materials with high specific energy density, and organic compounds with structural diversity [15–18]. Layered vanadic oxides (V_2O_5) have been extensively explored as promising cathode materials because they possess a upper voltage and a high-capacity as well as a large interlayer distance providing sufficient space for the Zn^{2+} intercalation/extraction [15,19–20]. Nevertheless, V_2O_5 suffers from issues of low diffusion coefficient of Zn^{2+} and structural deterioration during cycling, leading to poor rate capability and short life span. To ensure fast reversible (de)intercalation of Zn^{2+} and long cyclic life, a great number of works have been devoted to pre-intercalate large cations (such as Li^+, Ag^+, Zn^{2+}, Ca^{2+}, Mg^{2+}, Mn^{2+}, etc.) inside the V_2O_5 layers, which work as sturdy pillars to provide increased interlayer distance and prevent the structural destruction. For instance, $Zn_{0.25}V_2O_5{\cdot}nH_2O$ [21], $Mg_{0.34}V_2O_5{\cdot}0.84H_2O$ [22], $Na_{0.33}V_2O_5$ [23], as well as $K_{0.23}V_2O_5$ [24] were developed and they ex-

Corresponding authors: Peng-chao Zhang E-mail: zpc@dlmu.edu.cn; Xin-yu Wang E-mail: wangxinyu@dlmu.edu.cn; Qiong-qiong Lu E-mail: q.lu@ifw-dresden.de
© University of Science and Technology Beijing 2021

hibited excellent electrochemical performances due to the introduction of cations between vanadium oxygen layers. Similarly, the Ba^{2+} with the larger ionic radius also can act as "pillars" between vanadium oxygen layers. Meanwhile, divalent Ba^{2+} ions can combine with oxygen atoms forming stronger ionic bonds to bind the layers together in contrast to monovalent alkali cations (such as Li^+, Na^+, K^+), which can effectively prevent structural collapse. Due to these advantages, the Ba^{2+} intercalated V_2O_5 cathode material is meaningful to explore and expected to show prominent electrochemical performance in ZIBs.

In this work, we successfully fabricated $Ba_{0.23}V_2O_5{\cdot}1.1H_2O$ (BaVO) cathode material by a facile hydrothermal method, which exhibits reversible zinc storage and remarkable performance in ZIBs. Pre-intercalating Ba^{2+} and H_2O into the interlayer enhances the framework stability, enlarges interlayer spacing to 1.31 nm, and simultaneously reduces part of V^{5+} to V^{4+} on account of the charge compensation, which improves the electrical conductivity and ion diffusion ability of the prepared cathode materials. In conclusion, layered BaVO nanobelts exhibited a high initial discharge capacity of 378 $mAh{\cdot}g^{-1}$ at current density of 0.1 $A{\cdot}g^{-1}$, an excellent rate capability (e. g., 172 $mAh{\cdot}g^{-1}$ at a high current density of 5 $A{\cdot}g^{-1}$), and an extraordinary cyclic durability with the capacity only decreased by 7% after 2000 cycles. The excellent performance of the BaVO nanobelts cathode results from the increased interlayer distance by the introduction of Ba^{2+} and H_2O, which enables impressive ion diffusion rate of 0.233×10^{-8} to 2.97×10^{-8} $cm^2{\cdot}s^{-1}$ transcending most of the current hydrated-vanadate-based cathodes in ZIBs.

2. Experimental

2.1. Materials

Commercial vanadium pentoxide V_2O_5 (purity ≥ 99.7wt%) was purchased from Saren Chemical Technology Co., Ltd., China. Barium nitrate $Ba(NO_3)_2$ (purity ≥ 99.5wt%) was purchased from Xiya Reagent Co., Ltd., China. Hydrogen peroxide H_2O_2 (30wt%) was obtained from Tianjin Fengchuan Chemical Reagent Science & Technology Co., Ltd., China. Zn foils (purity ≥ 99wt%) were obtained from Sigma-Aldrich, USA. $Zn(CF_3SO_3)_2$ (purity ≥ 98wt%) was bought from Alfa Aesar, UK.

2.2. Preparation of BaVO nanobelts

In the process of preparing BaVO nanobelts, 0.827 g of $Ba(NO_3)_2$ was dispersed into 60 mL deionized water and continuously stirred at room temperature. After that, 4 mL of H_2O_2 (30wt%) was added drop by drop to 0.304 g of commercial V_2O_5 under vigorous stirring, initiating a reaction accompanied by oxygen evolution. Then, the mixture was poured into the above $Ba(NO_3)_2$ solution with electromagnetic stirring for 1 h, and the color of final mixture turned brown. Subsequently, the mixture was transferred to a reaction kettle, then it was heated to 180°C and maintained at the constant temperature for 24 h. The resultant composition was collected by centrifugation and washed several times with deionized water. Finally, the obtained materials were dried at 80°C for 12 h.

2.3. Material characterization

The morphology and elemental information of as-prepared BaVO nanobelts were investigated by the field-emission scanning electron microscopy (SEM, SUPRA 55 SAPPHIRE) equipped with energy dispersive X-ray spectroscopy. Further structural and crystalline characterization were characterized by transmission electron microscope (TEM) using JEM2100F. X-ray diffraction (XRD) was performed to confirm the phase structure of the obtained BaVO nanobelts on a Rigaku D/Max-3A with Co K_α radiation. Fourier transform infrared spectroscopy (FTIR) spectrum from 400 to 3000 cm^{-1} was recorded by a PerkinElmer FTIR spectrometer. X-ray photoelectron spectroscopy (XPS) was tested to investigate the composition and element valence states of the as-prepared BaVO materials using PerkinElmer PHI 1600 ESCA with a radiation source of Al. The thermogravimetric (TG) analysis from 30 to 600°C under argon atmosphere was collected by the NETZSCH STA 449 F3. The proportion of each element (Ba, V, O) in the as-prepared materials was determined by inductively coupled plasma optical emission spectroscopy (ICP-OES, Agilent 511).

2.4. Electrochemical measurements

ZIBs were assembled with BaVO and zinc foil as the cathode and anode, while 3 M $Zn(CF_3SO_3)_2$ aqueous solution and filter paper were used as the electrolyte and the separator. The assembly of ZIBs was performed in air. Cyclic voltammetry (CV) curves and electrochemical impedance spectroscopy (EIS) were tested with a CHI660E electrochemical workstation (CHI Instruments). The electrochemical performance of the assembled batteries was performed on the LAND CT2001 battery testing system. In the galvanostatic intermittent titration technique (GITT) experiments, the batteries operated at a current density of 0.2 $A{\cdot}g^{-1}$ for 7 min, followed by a relaxation time of 1 h.

3. Results and discussion

The preparation of BaVO nanobelts was through a typical hydrothermal synthesis method, and the crystal structure and phase purify of the obtained BaVO nanobelts was confirmed by XRD measurement. As Fig. 1(a) illustrates, all the diffraction peaks of XRD pattern could be indexed by $V_2O_5{\cdot}3H_2O$ (JCPDS No. 07-0332), and the XRD pattern of BaVO is similar to the previously reported literatures such as $Mg_{0.34}V_2O_5{\cdot}0.84H_2O$ [22], $Mn_{0.15}V_2O_5{\cdot}nH_2O$ [25] and Al–VOH

[26]. A little amount of V_2O_5 was also indexed and may be attributed to an incomplete reaction. The strongest peak locating at 2θ of ~6.75° corresponds to a large interlayer distance (d) of 1.31 nm, which is much larger than the parent material of $V_2O_5{\cdot}3H_2O$ (VOH). It is obvious that the introduction of Ba^{2+} and H_2O together increases the interlayer distance of V_2O_5 and keeps the integrality of VOH structure [22]. Such a large spacing would provide feasible access for the insertion/extraction of Zn^{2+}, which is helpful to improve the electrochemical performance of cathode materials. The FTIR spectrum characterization of the BaVO nanobelts is exhibited in Fig. 1(b). A series of absorption peaks appear at 812, 1002, 1408, and 1622 cm^{-1}, which are caused by various vibration modes of V–O–V, V=O, and H–O–H, respectively, in agreement with previous reports [27–28].

To further prove the intercalation of Ba^{2+} and confirm the oxidation state of vanadium in the BaVO nanobelts, XPS test was performed. Fig. 2(a) exhibits the full scan spectrum, and

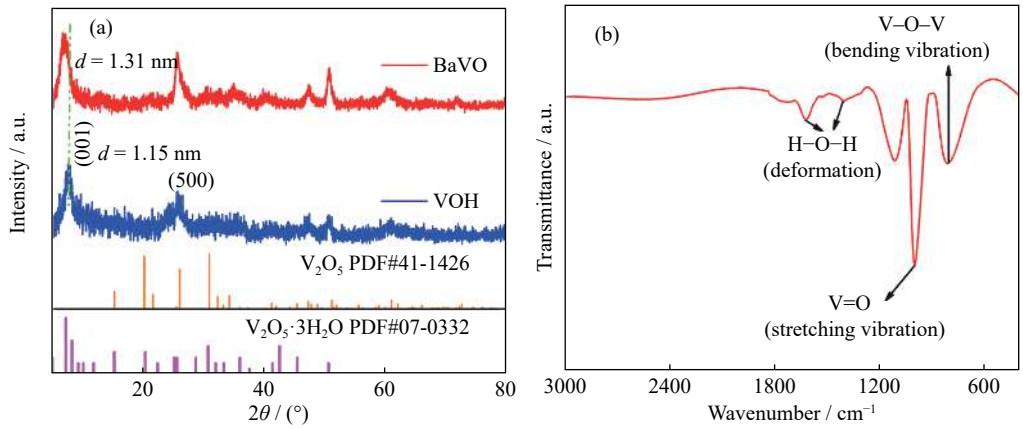

Fig. 1. (a) XRD pattern and (b) FTIR spectrum of the BaVO nanobelt.

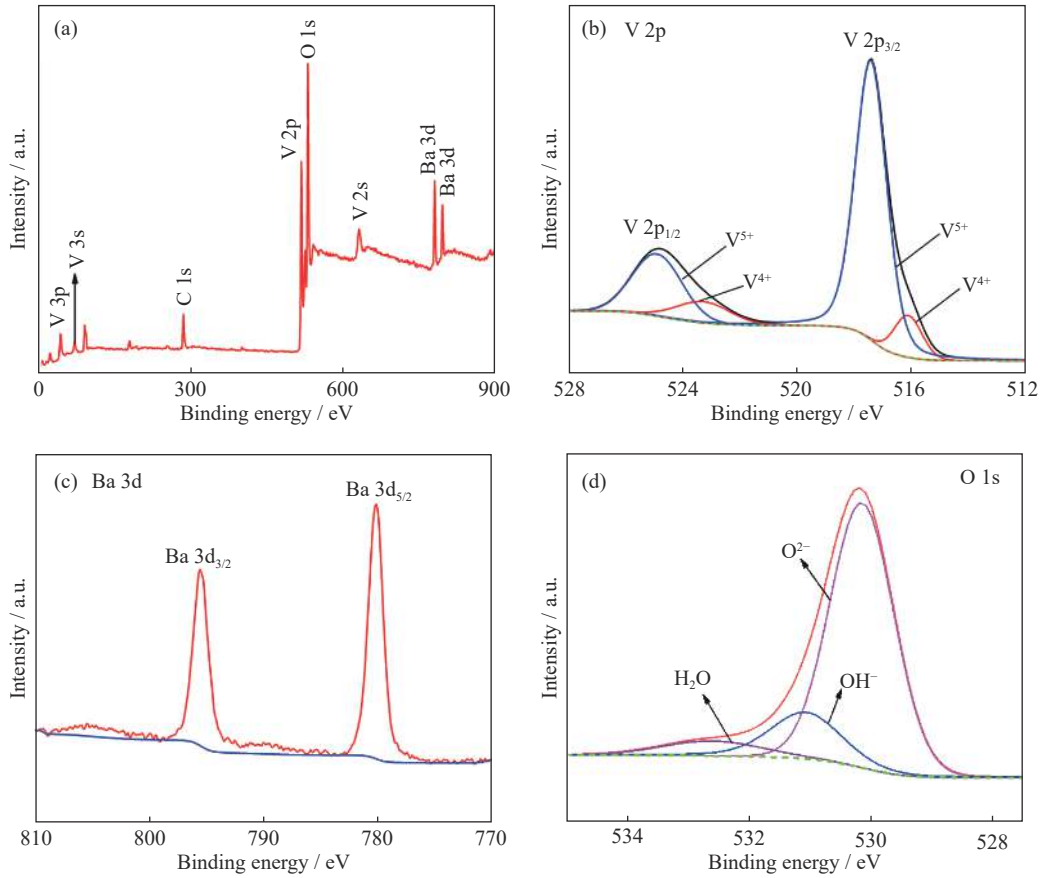

Fig. 2. XPS survey spectrum of the BaVO nanobelts: (a) full scan spectrum; high resolution of (b) V 2p spectrum, (c) Ba 3d spectrum, and (d) O 1s spectrum.

elements V, O, and Ba are present, confirming the successful introduction of Ba in the sample of the BaVO nanobelts. After peak fitting, a strong peak and a small shoulder peak in the V $2p_{3/2}$ spectrum appear and the peak positions are at 517.4 and 524.9 eV, assigning to V^{5+} and V^{4+}, respectively. In the V $2p_{1/2}$ spectrum, the peaks at 516.1 and 523.3 eV are ascribed to V^{5+} and V^{4+} (Fig. 2(b)) [29–31]. A small amount of vanadium is reduced due to charge compensation after pre-intercalating Ba^{2+}. The co-existence of V^{4+} and V^{5+} could make the cathode material higher electronic conductivity and excellent electrochemical reactivity according to the previous report [32]. The Ba $3d_{5/2}$ and Ba $3d_{3/2}$ spectrum located at 780.2 and 795.6 eV assign to Ba^{2+}, further confirming the successful intercalation of Ba^{2+} (Fig. 2(c)) [33]. In the O 1s spectrum (Fig. 2(d)), the O peak is fitted into three sub-peaks, whose binding energies are at 530.2, 531.1, and 532.6 eV assigned to lattice oxygen bonding with vanadium (O^{2-}), material surface adsorbed oxygen species (OH^-), and inserted H_2O molecules, respectively [33–35].

In order to detect the amount of structural water molecules, thermogravimetric (TG) analysis was further conducted (Fig. 3). The weight losses of samples are due to the vaporization of surface adsorption water (less than 100°C) and lattice water (100–400°C). The elemental compositions were characterized by ICP-OES (Table 1), the mole ratio of Ba and V in BaVO is about 1:8.67. According to the TG analysis and ICP-OES results, the stoichiometric formula of $Ba_{0.23}V_2O_5{\cdot}1.1H_2O$ is confirmed.

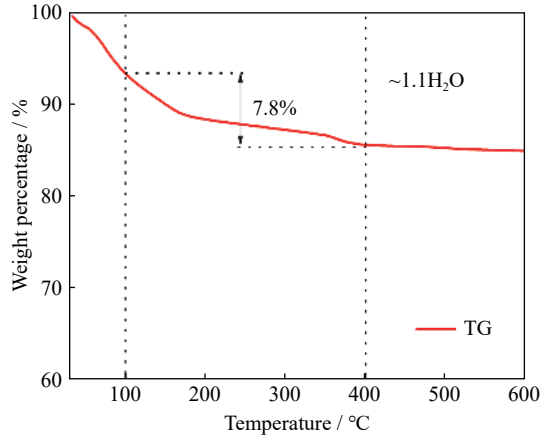

Fig. 3. TG result of the BaVO nanobelts.

Table 1. Elemental analysis of Ba and V in BaVO

Element	Mass content / ($mg{\cdot}kg^{-1}$)	Amount of substance / ($mmol{\cdot}kg^{-1}$)
Barium (Ba)	124359.3	907.7321
Vanadium (V)	401088.9	7864.4882

The morphology and elemental information of as-prepared BaVO nanobelts are characterized through SEM, TEM, and energy dispersive spectroscopy (EDS) analyses (Fig. 4). The BaVO nanobelts with high aspect ratio display a flat ribbon shape with several micrometers in length and 50–100 nm in width, as demonstrated in the SEM and TEM images (Figs. 4(a) and 4(c)). Notably, Barium element is validated again by the corresponding elemental mappings and EDS spectrum in Fig. 4(b), which further confirmed the successful synthesis of BaVO nanobelts and the homogeneous distribution of O, V, and Ba elements in the nanobelts. In addition, the polycrystalline property of the BaVO cathode material could be confirmed by selected area electron diffraction (SAED) diagram displayed in Fig. 4(d).

The electrochemical property of the pristine VOH and BaVO nanobelts is measured in ZIBs. Fig. 5(a) demonstrates the excellent rate capability of the BaVO nanobelts cathode, e.g., 378, 331, 297, 268, 228, 202, 185, and 170 $mAh{\cdot}g^{-1}$ at 0.1, 0.2, 0.5, 1, 2, 3, 4, and 5 $A{\cdot}g^{-1}$, correspondingly. It is much better than the unintercalated material of VOH. When the current density decreases from 5 to 0.1 $A{\cdot}g^{-1}$, the capacity recovers to 355 $mAh{\cdot}g^{-1}$, suggesting great electrochemical reversibility and excellent structural stability. On the basis of the charge/discharge profiles at different current densities (Fig. 5(b)), two typical voltage plateaus associated with Zn^{2+} insertion and extraction into BaVO are clearly observed in the discharge or charge curves. The Ragone plots in Fig. 5(c) show the energy vs. power densities comparing the BaVO cathode with previous ZIBs cathodes. As can be seen from the Ragone plots, when the power density is 40 $W{\cdot}kg^{-1}$, the energy density can reach 217 $Wh{\cdot}kg^{-1}$ for BaVO cathode. Even at an ultrahigh power density of about 1997 $W{\cdot}kg^{-1}$, the energy density can reach a very appreciable value of 96 $Wh{\cdot}kg^{-1}$. Obviously, the performance of BaVO cathode is better than those of reported vanadium composite cathodes used in ZIBs, such as $Zn_3V_2O_7(OH)_2$ [36], $NH_4V_4O_{10}$ [37], VS_2 [38], $Na_3V_2(PO_4)_3$ [39], $Ag_{0.33}V_2O_5$ [40], and LiV_3O_8 [41].

The cycling performance of the assembled ZIBs under various current densities was also evaluated to further demonstrate the effect of the Ba^{2+} and intermolecular water. As explicitly shown in Fig. 6(a), the BaVO cathode delivers a high initial capacity of 271 $mAh{\cdot}g^{-1}$ at current density of 1 $A{\cdot}g^{-1}$ and the capacity retention rate is close to 100% after 100 cycles, which is superior compared with that of the pristine VOH cathode (209 $mAh{\cdot}g^{-1}$, 86%). Fig. 6(b) shows curves of the corresponding differential capacitances (dQ/dV) at the selected cycles. The two pairs of broad peaks produced

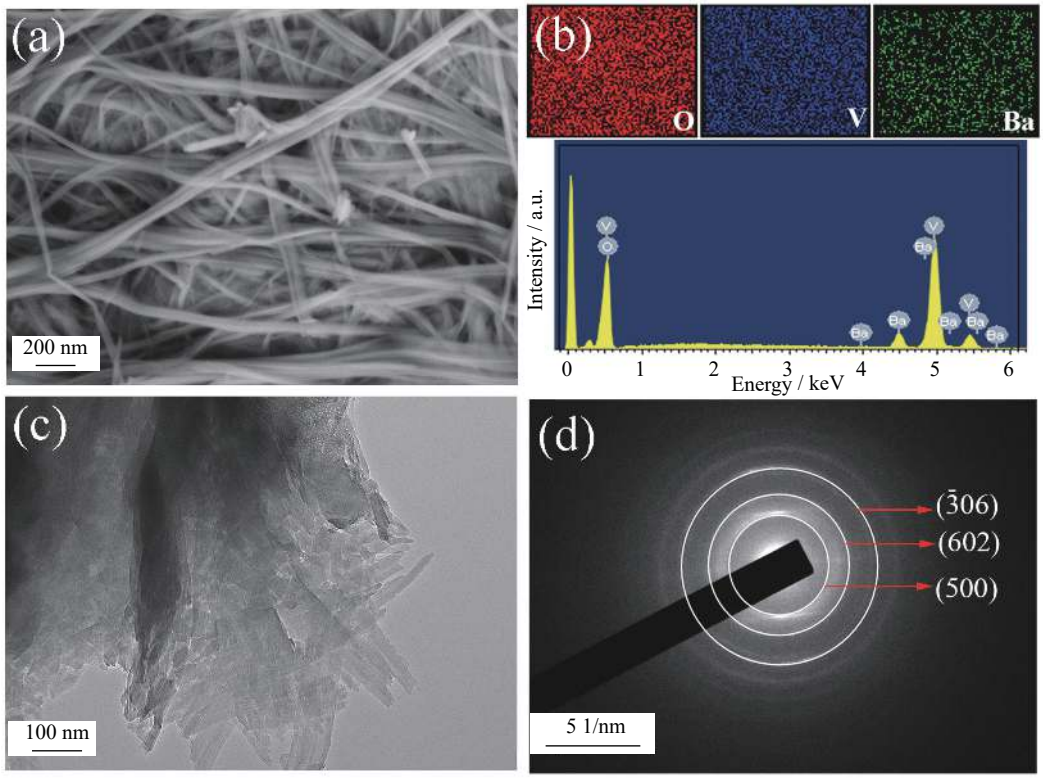

Fig. 4. Structural and morphological characterization of BaVO nanobelts: (a) SEM image; (b) corresponding elemental mappings and EDS spectrum; (c) TEM image; (d) SAED image.

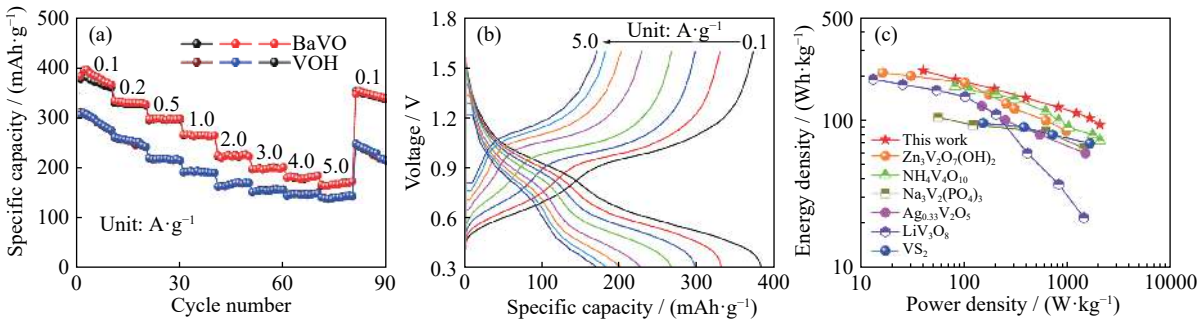

Fig. 5. (a) Rate capability and (b) corresponding charge/discharge profiles of BaVO with various current densities; (c) Ragone plots of the BaVO nanobelts comparing with other materials reported in the related literatures.

by the insertion–extraction reaction have good overlap and little offset. This result demonstrated the high reversibility of the BaVO cathode. Even at 5 $A \cdot g^{-1}$ (Fig. 6(c)), the BaVO cathode remains a stable capacity of 172 $mAh \cdot g^{-1}$ after 2000 repetitive cycles (only 7% reduction). The average coulombic efficiency is generally stable around 100%, which effectively manifests that the BaVO cathode has the great reversibility in the long-term charge–discharge tests. In a sharp contrast, the pristine VOH cathode only showed a capacity retention of 62%. These results demonstrated that the intercalation of Ba^{2+} and H_2O not only enhances the reversibility, but also increases the framework stability.

EIS was performed to analyze the impedance of BaVO cathode before cycling. Fig. 7 presents the Nyquist plot and the corresponding equivalent circuit. Thereinto, the charge transfer resistance (R_2) of batteries represents the diameter of the semicircle at the high frequency region of the Nyquist plot [42–43]. The calculated R_2 value of the BaVO electrode before cycling is 128.3 Ω and lower than the previous materials such as $K_{0.23}V_2O_5$ [24], $Ni_{0.25}V_2O_5 \cdot nH_2O$ [27], $Li_xV_2O_5 \cdot nH_2O$ [44], which indicates the enhanced conductivity.

The electrochemical kinetics of the BaVO electrode was investigated by cyclic voltammograms method. The similar shapes CV curves of the BaVO cathode tested at different scan rates (0.1–1.0 $mV \cdot s^{-1}$) with a voltage window (0.3–1.6

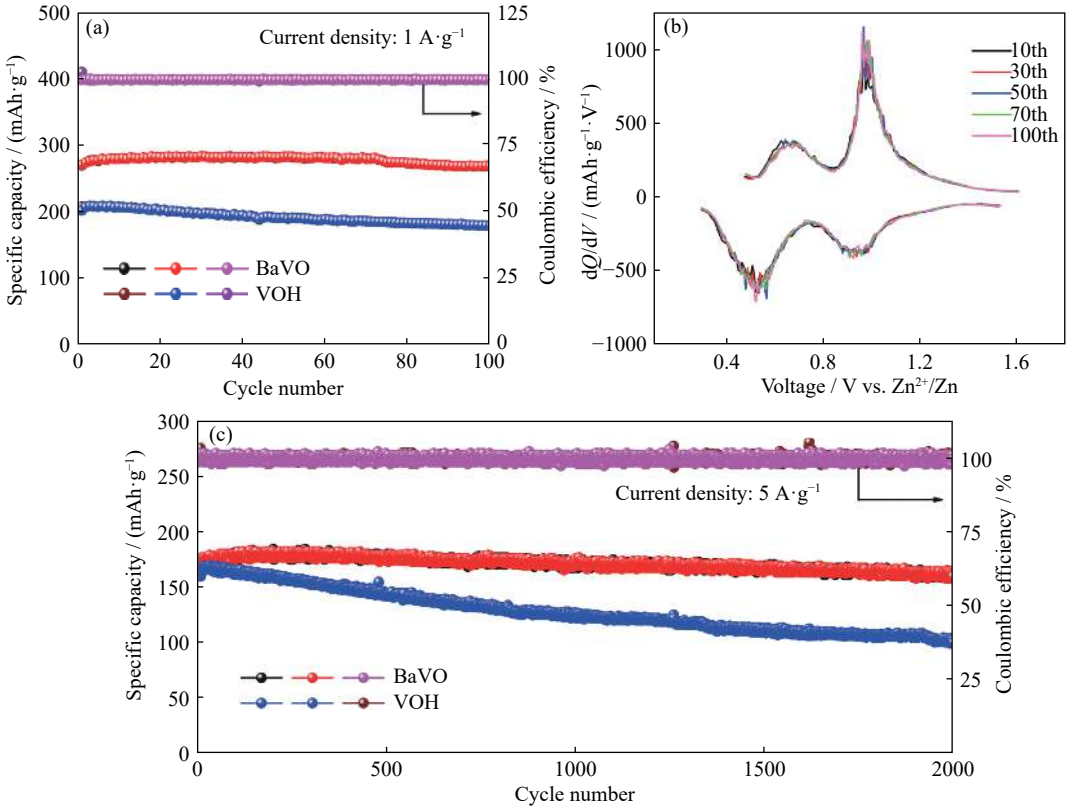

Fig. 6. (a) Cycle performance of BaVO nanobelt electrode at the current density of 1 A·g^{-1} for 100 cycles; (b) corresponding dQ/dV curves of the selected cycles at 1 A·g^{-1}; (c) cycle performance of BaVO nanobelt electrode at 5 A·g^{-1} for 2000 cycles.

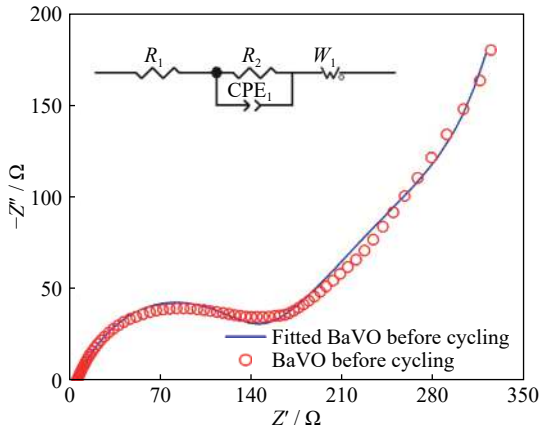

Fig. 7. Nyquist impedance plot of ZIBs based on BaVO with frequency range from 100 kHz to 100 mHz (Z'—Real component of impedance; Z''—Imaginary component of impedance; R_1—Ohmic resistance; R_2—Charge transfer resistance; CPE$_1$—Nonideal double-layer capacitance; W_1—Warburg impedance).

V) are exhibited in Fig. 8(a). There are two pairs of diverse reduction/oxidation peaks at around 0.46/0.75 V and 0.85/1.1 V, suggesting that the intercalation/extraction processes of Zn^{2+} consist of two step reactions [30,45]. Meanwhile, it can be seen that the reduction/oxidation peaks are the same as the charge/discharge plateaus (Fig. 5(b)). In theory, there is a relationship between the peak current (i) and scan rate (v), which can be described by the equation [31,36]:

$$i = av^b \text{ or } \lg i = b\lg v + \lg a,$$

where a and b refer to parameters, and the b value can be calculated by linear fitting of the peak current at different scan rates. When b value is 0.5, the capacity is determined by the diffusion-controlled process. The b value is 1.0, suggesting the surface-controlled capacitive process determined. As shown in Fig. 8(b), the calculated b-values of peaks Ⅰ–Ⅳ are 0.64, 0.89, 0.77 and 0.85, respectively, which imply that the capacitive and diffusion-controlled processes simultaneously influence the electrochemical kinetics of the BaVO cathode [46]. Moreover, the contribution percentages of capacitive and diffusion-controlled processes at diverse scanning rates are calculated and given in Fig. 8(c). In the scanning rate range of 0.1–1 mV·s^{-1}, the ratios of capacitive contribution gradually increase from 58% to 82%, revealing that the corresponding redox reactions are dominated by the surface reaction rate instead of the ion diffusion speed [38,47–48].

To investigate more insight into the diffusion kinetics of the BaVO cathode, GITT is executed to calculate the diffusion coefficient of Zn^{2+} ($D_{Zn^{2+}}$). The GITT curves of BaVO electrode are shown in Fig. 9(a). The curves are in accord-

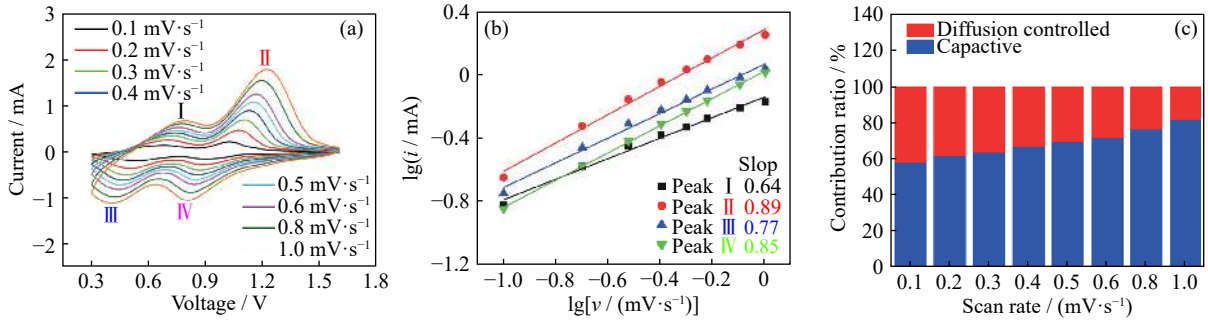

Fig. 8. (a) CV curves of the ZIBs based on the BaVO cathode at various scan rates; (b) *b*-values corresponding to the four peaks of CV curves during cycling in (a); (c) corresponding pseudo-capacitive contributions at disparate scan rates.

ance with the previously mentioned constant current charge–discharge profiles (Fig. 5(b)). The calculated $D_{Zn^{2+}}$ values are 0.233×10^{-8}–2.97×10^{-8} $cm^2 \cdot s^{-1}$ during the discharge process and 0.396×10^{-8}–2.06×10^{-8} $cm^2 \cdot s^{-1}$ during the charge process (Fig. 9(b)), which are comparable to the other previous V-based ZIBs cathodes [24,42].

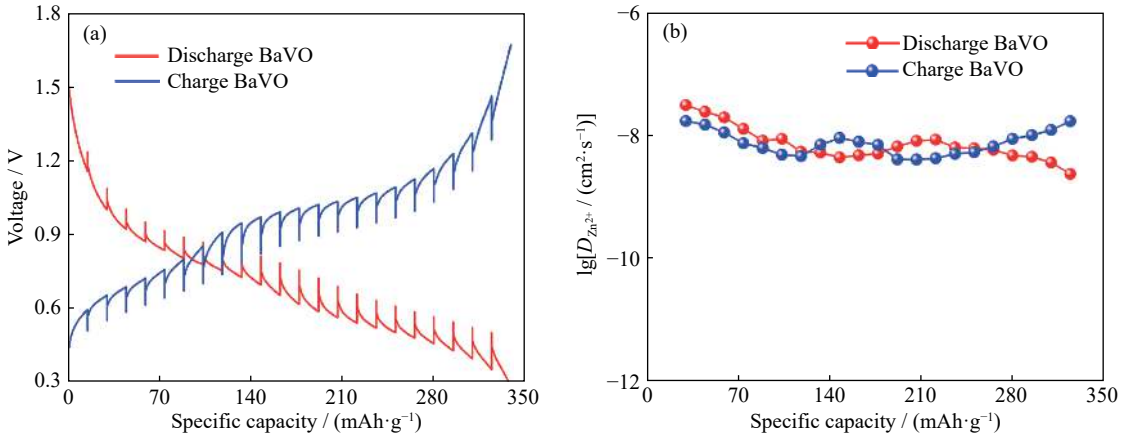

Fig. 9. (a) Charge/discharge GITT curves at 0.2 $A \cdot g^{-1}$ and (b) diffusion coefficient of Zn^{2+} for the BaVO cathode.

4. Conclusion

In summary, The BaVO nanobelts were successfully fabricated by a typical hydrothermal synthesis method and employed as the cathode for ZIBs. On account of the intercalation of Ba^{2+} and H_2O as pillars, the BaVO cathode possesses relatively large interlayer spacing and the highly stable structure. Consequently, the BaVO electrode delivers a high capacity of 378 $mAh \cdot g^{-1}$ at 0.1 $A \cdot g^{-1}$, long-term cyclic stability, high-capacity retention rate (only 7% reduction for 2000 cycles even at 5 $A \cdot g^{-1}$), and excellent rate performance. The superior electrochemical performance of BaVO cathode indicates that aqueous ZIBs based on the BaVO cathode has a wide potential application for the large-scale energy storage.

Acknowledgements

This work was supported by the National Natural Science Foundation of China (No. 21905037), the Doctoral research startup fund of Liaoning Province, China (No. 2020-BS-066), the China Postdoctoral Science Foundation (No. 2020M670719), and the Fundamental Research Funds for the Central Universities (No. 3132019328). Qiong-qiong Lu and Ai-kai Yang acknowledge the financial support from China Scholarship Council (CSC).

References

[1] N. Nitta, F.X. Wu, J.T. Lee, and G. Yushin, Li-ion battery materials: Present and future, *Mater. Today*, 18(2015), No. 5, p. 252.

[2] L.Y. Shao, S.G. Wang, F.D. Wu, X.Y. Shi, Z.P. Sun, and Y.X. Tang, Pampas grass-inspired FeOOH nanobelts as high performance anodes for sodium ion batteries, *J. Energy Chem.*, 54(2021), p. 138.

[3] J.M. Tarascon and M. Armand, Issues and challenges facing rechargeable lithium batteries, *Nature*, 414(2001), No. 6861, p. 359.

[4] X.Y. Wang, L.W. Ma, P.C. Zhang, H.Y. Wang, S. Li, S.J. Ji, Z.S. Wen, and J.C. Sun, Vanadium pentoxide nanosheets as cathodes for aqueous zinc-ion batteries with high rate capability and long durability, *Appl. Surf. Sci.*, 502(2020), art. No. 144207.

[5] M.S. Zhu, J.P. Hu, Q.Q. Lu, H.Y. Dong, D.D. Karnaushenko,

C. Becker, D. Karnaushenko, Y. Li, H.M. Tang, Z. Qu, J. Ge, and O.G. Schmidt, A patternable and *in situ* formed polymeric zinc blanket for a reversible zinc anode in a skin-mountable microbattery, *Adv. Mater.*, 33(2021), No. 8, art. No. 2007497.

[6] S. Liu, G.L. Pan, G.R. Li, and X.P. Gao, Copper hexacyanoferrate nanoparticles as cathode material for aqueous Al-ion batteries, *J. Mater. Chem. A*, 3(2015), No. 3, p. 959.

[7] P. Canepa, G. Sai Gautam, D.C. Hannah, R. Malik, M. Liu, K.G. Gallagher, K.A. Persson, and G. Ceder, Odyssey of multivalent cathode materials: Open questions and future challenges, *Chem. Rev.*, 117(2017), No. 5, p. 4287.

[8] T. Hu, Z.Y. Feng, Y.F. Zhang, Y.Y. Liu, J.J. Sun, J.Q. Zheng, H.M. Jiang, P. Wang, X.Y. Dong, and C.G. Meng, "Double guarantee mechanism" of Ca^{2+}-intercalation and rGO-integration ensures hydrated vanadium oxide with high performance for aqueous zinc-ion batteries, *Inorg. Chem. Front.*, 8(2021), No. 1, p. 79.

[9] Y.H. Du, X.Y. Wang, and J.C. Sun, Tunable oxygen vacancy concentration in vanadium oxide as mass-produced cathode for aqueous zinc-ion batteries, *Nano Res.*, 14(2021), No. 3, p. 754.

[10] X.Y. Wang, X.H. Qin, Q.Q. Lu, M.M. Han, A. Omar, and D. Mikhailova, Mixed phase sodium manganese oxide as cathode for enhanced aqueous zinc-ion storage, *Chin. J. Chem. Eng.*, 28(2020), No. 8, p. 2214.

[11] Y. Dong, M. Jia, Y.Y. Wang, J.Z. Xu, Y.C. Liu, L.F. Jiao, and N. Zhang, Long-life zinc/vanadium pentoxide battery enabled by a concentrated aqueous $ZnSO_4$ electrolyte with proton and zinc ion co-intercalation, *ACS Appl. Energy Mater.*, 3(2020), No. 11, p. 11183.

[12] N. Zhang, Y. Dong, Y.Y. Wang, Y.X. Wang, J.J. Li, J.Z. Xu, Y.C. Liu, L.F. Jiao, and F.Y. Cheng, Ultrafast rechargeable zinc battery based on high-voltage graphite cathode and stable non-aqueous electrolyte, *ACS Appl. Mater. Interfaces*, 11(2019), No. 36, p. 32978.

[13] N. Zhang, X.Y. Chen, M. Yu, Z.Q. Niu, F.Y. Cheng, and J. Chen, Materials chemistry for rechargeable zinc-ion batteries, *Chem. Soc. Rev.*, 49(2020), No. 13, p. 4203.

[14] L. Xu, Y. Zhang, J. Zheng, H. Jiang, T. Hu, and C. Meng, Ammonium ion intercalated hydrated vanadium pentoxide for advanced aqueous rechargeable Zn-ion batteries, *Mater. Today Energy*, 18(2020), art. No. 100509.

[15] S.D. Liu, L. Kang, J.M. Kim, Y.T. Chun, J. Zhang, and S.C. Jun, Recent advances in vanadium-based aqueous rechargeable zinc-ion batteries, *Adv. Energy Mater.*, 10(2020), No. 25, art. No. 2000477.

[16] Y.R. Wang, C.X. Wang, Z.G. Ni, Y.M. Gu, B.L. Wang, Z.W. Guo, Z. Wang, D. Bin, J. Ma, and Y.G. Wang, Binding zinc ions by carboxyl groups from adjacent molecules toward long-life aqueous zinc–organic batteries, *Adv. Mater.*, 32(2020), No. 16, art. No. 2000338.

[17] G. Zampardi and F. La Mantia, Prussian blue analogues as aqueous Zn-ion batteries electrodes: Current challenges and future perspectives, *Curr. Opin. Electrochem.*, 21(2020), p. 84.

[18] M.Q. Liu, Q.H. Zhao, H. Liu, J.L. Yang, X. Chen, L.Y. Yang, Y.H. Cui, W.Y. Huang, W.G. Zhao, A.Y. Song, Y.T. Wang, S.X. Ding, Y.L. Song, G.Y. Qian, H.B. Chen, and F. Pan, Tuning phase evolution of β-MnO_2 during microwave hydrothermal synthesis for high-performance aqueous Zn ion battery, *Nano Energy*, 64(2019), art. No. 103942.

[19] Y.Y. Liu, Z.H. Pan, D. Tian, T. Hu, H.M. Jiang, J. Yang, J.J. Sun, J.Q. Zheng, C.G. Meng, and Y.F. Zhang, Employing "one for two" strategy to design polyaniline-intercalated hydrated vanadium oxide with expanded interlayer spacing for high-performance aqueous zinc-ion batteries, *Chem. Eng. J.*, 399(2020), art. No. 125842.

[20] Y.F. Zhang, H.M. Jiang, L. Xu, Z.M. Gao, and C.G. Meng, Ammonium vanadium oxide $[(NH_4)_2V_4O_9]$ sheets for high capacity electrodes in aqueous zinc ion batteries, *ACS Appl. Energy Mater.*, 2(2019), No. 11, p. 7861.

[21] D.P. Kundu, B.D. Adams, V. Duffort, S.H. Vajargah, and L.F. Nazar, A high-capacity and long-life aqueous rechargeable zinc battery using a metal oxide intercalation cathode, *Nat. Energy*, 1(2016), art. No. 16119.

[22] F.W. Ming, H.F. Liang, Y.J. Lei, S. Kandambeth, M. Eddaoudi, and H.N. Alshareef, Layered $Mg_xV_2O_5{\cdot}nH_2O$ as cathode material for high-performance aqueous zinc ion batteries, *ACS Energy Lett.*, 3(2018), No. 10, p. 2602.

[23] P. He, G.B. Zhang, X.B. Liao, M.Y. Yan, X. Xu, Q.Y. An, J. Liu, and L.Q. Mai, Sodium ion stabilized vanadium oxide nanowire cathode for high-performance zinc-ion batteries, *Adv. Energy Mater.*, 8(2018), No. 10, art. No. 1702463.

[24] W.W. Zhang, C. Tang, B.X. Lan, L.N. Chen, W. Tang, C.L. Zuo, S.J. Dong, Q.Y. An, and P. Luo, $K_{0.23}V_2O_5$ as a promising cathode material for rechargeable aqueous zinc ion batteries with excellent performance, *J. Alloys Compd.*, 819(2020), art. No. 152971.

[25] H.B. Geng, M. Cheng, B. Wang, Y. Yang, Y.F. Zhang, and C.C. Li, Electronic structure regulation of layered vanadium oxide via interlayer doping strategy toward superior high-rate and low-temperature zinc-ion batteries, *Adv. Funct. Mater.*, 30(2020), No. 6, art. No. 1907684.

[26] J.Q. Zheng, C.F. Liu, M. Tian, X.X. Jia, E.P. Jahrman, G.T. Seidler, S.Q. Zhang, Y.Y. Liu, Y.F. Zhang, C.G. Meng, and G.Z. Cao, Fast and reversible zinc ion intercalation in Al-ion modified hydrated vanadate, *Nano Energy*, 70(2020), art. No. 104519.

[27] J.W. Li, K. McColl, X.K. Lu, S. Sathasivam, H.B. Dong, L.Q. Kang, Z.N. Li, S.Y. Zhao, A.G. Kafizas, R. Wang, D.J.L. Brett, P.R. Shearing, F. Corà, G.J. He, C.J. Carmalt, and I.P. Parkin, Multi-scale investigations of δ-$Ni_{0.25}V_2O_5{\cdot}nH_2O$ cathode materials in aqueous zinc-ion batteries, *Adv. Energy Mater.*, 10(2020), No. 15, art. No. 2000058.

[28] Y.F. Zhang, J.Q. Zheng, Y.F. Zhao, T. Hu, Z.M. Gao, and C.G. Meng, Fabrication of V_2O_5 with various morphologies for high-performance electrochemical capacitor, *Appl. Surf. Sci.*, 377(2016), p. 385.

[29] Y.H. Du, X.Y. Wang, J.Z. Man, and J.C. Sun, A novel organic–inorganic hybrid V_2O_5@polyaniline as high-performance cathode for aqueous zinc-ion batteries, *Mater. Lett.*, 272(2020), art. No. 127813.

[30] X.H. Qin, X.Y. Wang, J.C. Sun, Q.Q. Lu, A. Omar, and D. Mikhailova, Polypyrrole wrapped V_2O_5 nanowires composite for advanced aqueous zinc-ion batteries, *Front. Energy Res.*, 8(2020), art. No. 199.

[31] N. Zhang, Y. Dong, M. Jia, X. Bian, Y.Y. Wang, M.D. Qiu, J.Z. Xu, Y.C. Liu, L.F. Jiao, and F.Y. Cheng, Rechargeable aqueous Zn–V_2O_5 battery with high energy density and long cycle life, *ACS Energy Lett.*, 3(2018), No. 6, p. 1366.

[32] Y. Xu, X.S. Han, L. Zheng, W.S. Yan, and Y. Xie, Pillar effect on cyclability enhancement for aqueous lithium ion batteries: A new material of β-vanadium bronze $M_{0.33}V_2O_5$ (M = Ag, Na) nanowires, *J. Mater. Chem.*, 21(2011), No. 38, p. 14466.

[33] X. Wang, B.J. Xi, X.J. Ma, Z.Y. Feng, Y.X. Jia, J.K. Feng, Y.T. Qian, and S.L. Xiong, Boosting zinc-ion storage capability by effectively suppressing vanadium dissolution based on robust layered barium vanadate, *Nano Lett.*, 20(2020), No. 4, p. 2899.

[34] F.J. Tang, W.J. Zhou, M.F. Chen, J.Z. Chen, and J.L. Xu, Flexible free-standing paper electrodes based on reduced graphene oxide/δ-$Na_xV_2O_5{\cdot}nH_2O$ nanocomposite for high-performance aqueous zinc-ion batteries, *Electrochim. Acta*, 328(2019), art. No. 135137.

[35] T.Y. Wei, Q. Li, G.Z. Yang, and C.X. Wang, Highly reversible and long-life cycling aqueous zinc-ion battery based on ultrathin $(NH_4)_2V_{10}O_{25}{\cdot}8H_2O$ nanobelts, *J. Mater. Chem. A*, 6(2018), No. 41, p. 20402.

[36] C. Xia, J. Guo, Y.J. Lei, H.F. Liang, C. Zhao, and H.N. Alshareef, Rechargeable aqueous zinc-ion battery based on porous framework zinc pyrovanadate intercalation cathode, *Adv. Mater.*, 30(2018), No. 5, art. No. 1705580.

[37] G.Z. Yang, T.Y. Wei, and C.X. Wang, Self-healing lamellar structure boosts highly stable zinc-storage property of bilayered vanadium oxides, *ACS Appl. Mater. Interfaces*, 10(2018), No. 41, p. 35079.

[38] P. He, M.Y. Yan, G.B. Zhang, R.M. Sun, L.N. Chen, Q.Y. An, and L.Q. Mai, Layered VS_2 nanosheet-based aqueous Zn ion battery cathode, *Adv. Energy Mater.*, 7(2017), No. 11, art. No. 1601920.

[39] G.L. Li, Z. Yang, Y. Jiang, C.H. Jin, W. Huang, X.L. Ding, and Y.H. Huang, Towards polyvalent ion batteries: A zinc-ion battery based on NASICON structured $Na_3V_2(PO_4)_3$, *Nano Energy*, 25(2016), p. 211.

[40] B.X. Lan, Z. Peng, L.N. Chen, C. Tang, S.J. Dong, C. Chen, M. Zhou, C. Chen, Q.Y. An, and P. Luo, Metallic silver doped vanadium pentoxide cathode for aqueous rechargeable zinc ion batteries, *J. Alloys Compd.*, 787(2019), p. 9.

[41] M.H. Alfaruqi, V. Mathew, J.J. Song, S. Kim, S. Islam, D.T. Pham, J. Jo, S. Kim, J.P. Baboo, Z.L. Xiu, K.S. Lee, Y.K. Sun, and J. Kim, Electrochemical zinc intercalation in lithium vanadium oxide: A high-capacity zinc-ion battery cathode, *Chem. Mater.*, 29(2017), No. 4, p. 1684.

[42] P. He, Y.L. Quan, X. Xu, M.Y. Yan, W. Yang, Q.Y. An, L. He, and L.Q. Mai, High-performance aqueous zinc-ion battery based on layered $H_2V_3O_8$ nanowire cathode, *Small*, 13(2017), No. 47, art. No. 1702551.

[43] X.W. Wu, Y.H. Li, Y.H. Xiang, Z.X. Liu, Z.Q. He, X.M. Wu, Y.J. Li, L.Z. Xiong, C.C. Li, and J. Chen, The electrochemical performance of aqueous rechargeable battery of $Zn/Na_{0.44}MnO_2$ based on hybrid electrolyte, *J. Power Sources*, 336(2016), p. 35.

[44] Y.Q. Yang, Y. Tang, G.Z. Fang, L.T. Shan, J.S. Guo, W.Y. Zhang, C. Wang, L.B. Wang, J. Zhou, and S.Q. Liang, Li^+ intercalated $V_2O_5{\cdot}nH_2O$ with enlarged layer spacing and fast ion diffusion as an aqueous zinc-ion battery cathode, *Energy Environ. Sci.*, 11(2018), No. 11, p. 3157.

[45] N. Zhang, M. Jia, Y. Dong, Y.Y. Wang, J.Z. Xu, Y.C. Liu, L.F. Jiao, and F.Y. Cheng, Hydrated layered vanadium oxide as a highly reversible cathode for rechargeable aqueous zinc batteries, *Adv. Funct. Mater.*, 29(2019), No. 10, art. No. 1807331.

[46] X.Y. Wang, L.W. Ma, and J.C. Sun, Vanadium pentoxide nanosheets *in-situ* spaced with acetylene black as cathodes for high-performance zinc-ion batteries, *ACS Appl. Mater. Interfaces*, 11(2019), No. 44, p. 41297.

[47] M.Y. Yan, P. He, Y. Chen, S.Y. Wang, Q.L. Wei, K.N. Zhao, X. Xu, Q.Y. An, Y. Shuang, Y.Y. Shao, K.T. Mueller, L.Q. Mai, J. Liu, and J.H. Yang, Water-lubricated intercalation in $V_2O_5{\cdot}nH_2O$ for high-capacity and high-rate aqueous rechargeable zinc batteries, *Adv. Mater.*, 30(2018), No. 1, art. No. 1703725.

[48] L.Y. Shao, J.Z. Hong, S.G. Wang, F.D. Wu, F. Yang, X.Y. Shi, and Z.P. Sun, Urchin-like FeS_2 hierarchitectures wrapped with N-doped multi-wall carbon nanotubes@rGO as high-rate anode for sodium ion batteries, *J. Power Sources*, 491(2021), art. No. 229627.